SUPPLEMENTARY INFORMATION

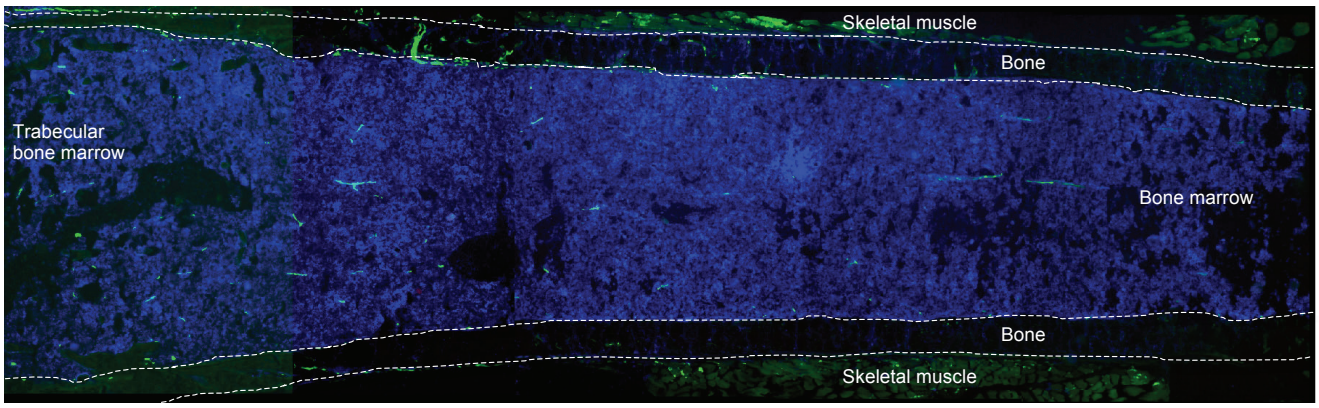

Supplementary Figure 1. **Distribution of GFP$^+$ cells in the bone marrow of *Nes-Gfp* transgenic mice**. Composite images at low magnification showing the distribution and low frequency of GFP$^+$ cells in the bone marrow of adult *Nes-Gfp* transgenic mice. Haematopoietic lineages (blue) have been identified with anti-Ter119, -Gr-1, -CD3e, -B220, -Mac-1 and -CD48 antibodies. Bone margins are indicated with dashed lines.

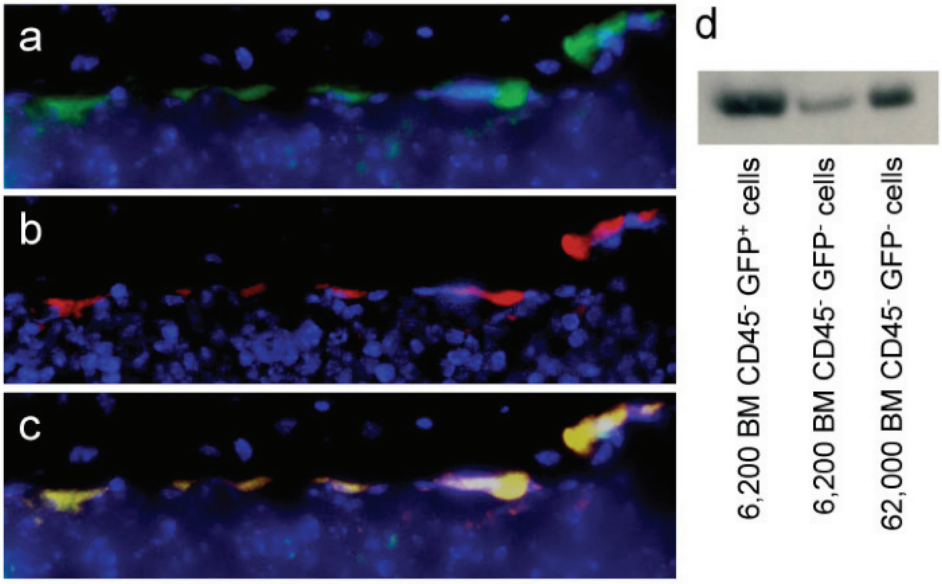

Supplementary Figure 2. **Expression of GFP in *Nes-Gfp* transgenic mice correlates with enriched expression of endogenous nestin**.
a-**c**, Immunohistochemistry of a femoral section from *Nes-Gfp* transgenic mice showing GFP^+ cells (**a**, green), distributed along the endosteum, that also stained positive using a polyclonal rabbit anti-nestin antibody (LifeSpan Biosciences) detected using the TSA amplification system (Perkin Elmer; **b**, red). **c**, Merged image. **a**-**c**, Nuclei have been stained with DAPI (blue). **d**, Representative Western blot (n = 4 mice) performed in lysates from sorted $CD45^-$ GFP^+ and $CD45^-$ GFP^- cells using a monoclonal anti-nestin antibody (clone Rat-401, Millipore). Immunoreactive proteins of molecular weight consistent with nestin are enriched in bone marrow (BM) $CD45^-$ GFP^+ cells when compared to the same or a 10-fold higher number of $CD45^-$ GFP^- cells.

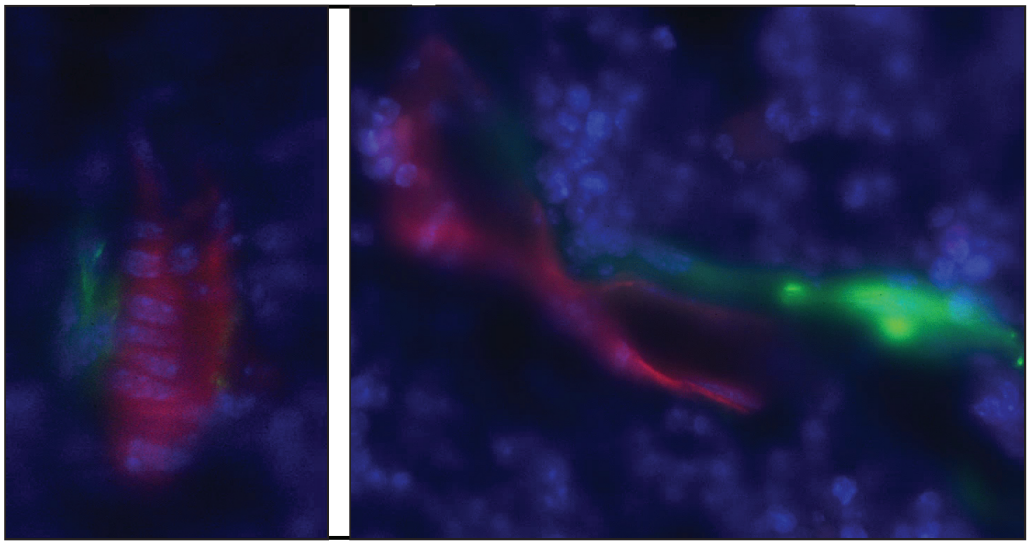

Supplementary Figure 3. **Illustrative movies from Z-stacks showing the peri-vascular distribution of bone marrow Nes:GFP$^+$ cells**. Movies from ~ 10 μm Z-stacks showing fluorescent signals from GFP (green), vascular endothelial cells immunostained with a biotinylated rat anti-CD31/PECAM monoclonal antibody (clone MEC13.3, BD Pharmingen) detected with the TSA amplification system (Perkin Elmer, red) and nuclei counterstained with DAPI (blue). Note how the shape of Nes:GFP$^+$ cells closely follows the contour of vascular endothelial cells (please click using Adobe® Acrobat® hand tool to play movies).

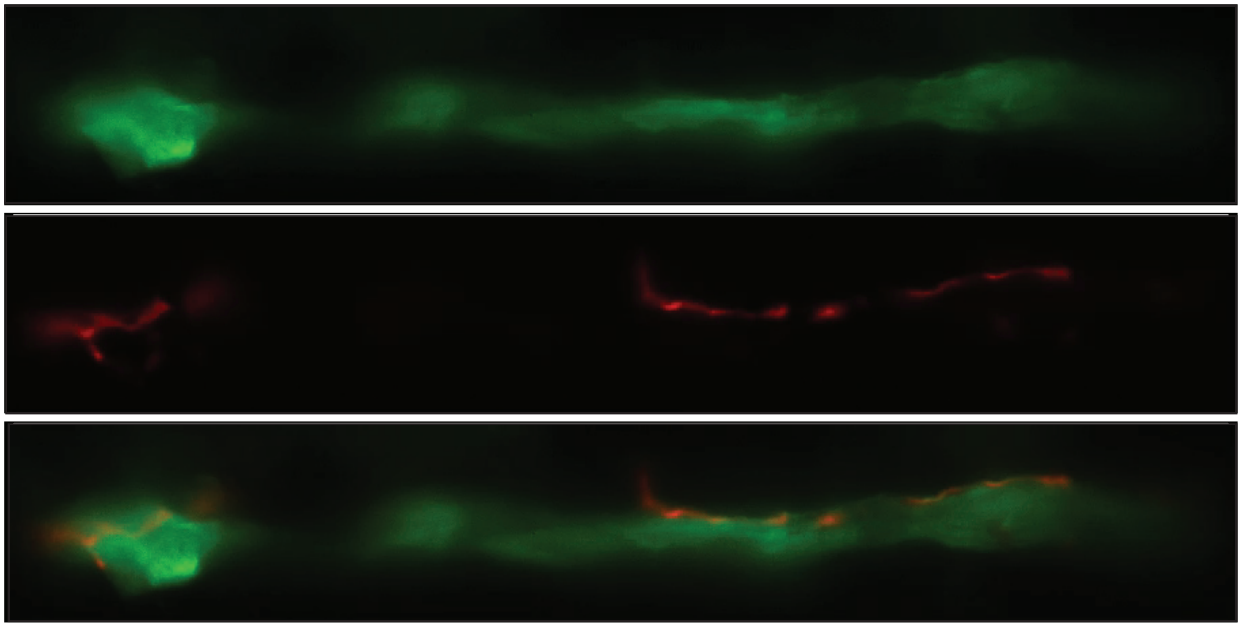

Supplementary Figure 4. **Illustrative movies from Z-stacks showing the close association between catecholaminergic nerve fibres and Nes:GFP^{+} cells in the bone marrow**. Movies from ~ 10 μm Z-stack shown in Fig. 1e (main paper) containing GFP fluorescence (upper panel, green), catecholaminergic nerve fibres immunostained with anti-tyrosine hydroxylase antibodies (middle panel, red) and merged fluorescence (lower panel).

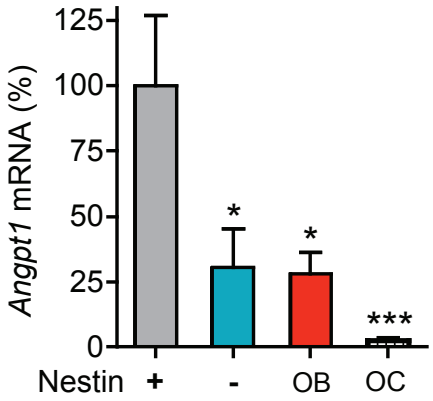

Supplementary Figure 5. Expression of *Angiopoietin-1* is significantly higher in CD45$^-$ Nes:GFP$^+$ cells than in other bone marrow stromal cells. Expression of *Angiopoietin-1* (*Angpt1*) was 3-4-fold higher in CD45$^-$ GFP$^+$ cells than in CD45$^-$ GFP$^-$ cells (sorted from the bone marrow of *Nes-Gfp* transgenic mice) and primary osteoblasts (OB), and > 40-fold higher than in primary osteoclasts (OC). Quantitative real-time RT-PCR. * $p < 0.05$; *** $p < 0.001$; unpaired two-tailed *t* test; n = 3-10. Error bars indicate SEM.

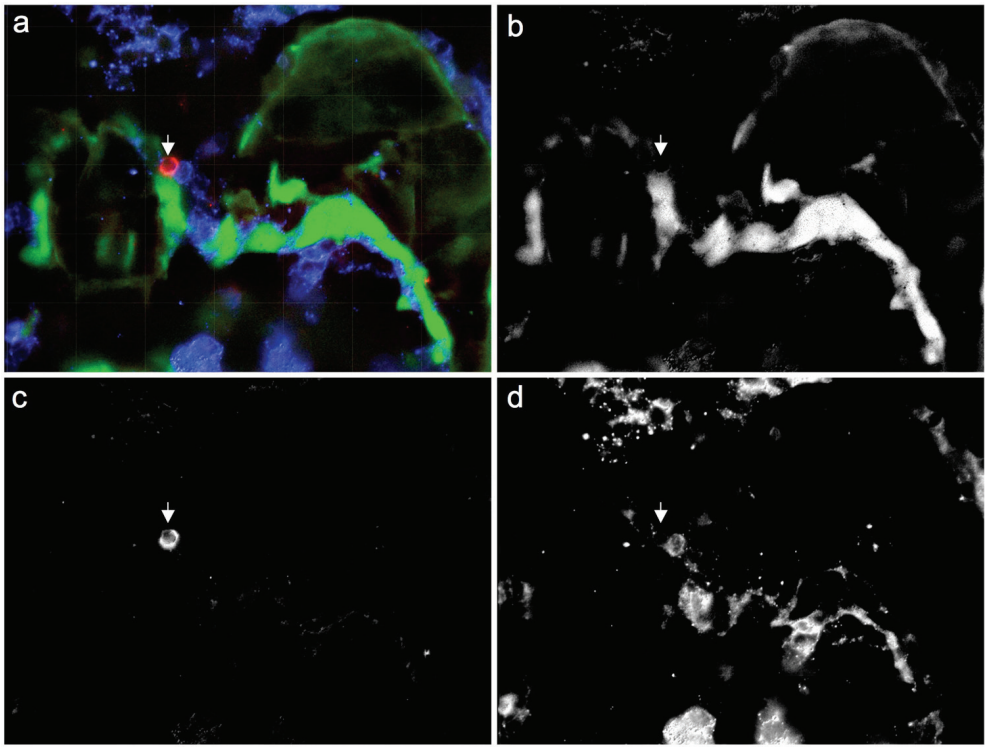

Supplementary Figure 6. Validation of HSC immunostaining.
Fig. 1j of the main paper (**a**) has been split here to show individual fluorescent signals from (**b**) GFP, (**c**) CD150, (**d**) CD48 and haematopoietic lineage markers to demonstrate that $CD150^{+}$ HSCs identified in our study (arrow points towards an example) were negative for CD48 and haematopoietic lineage markers.

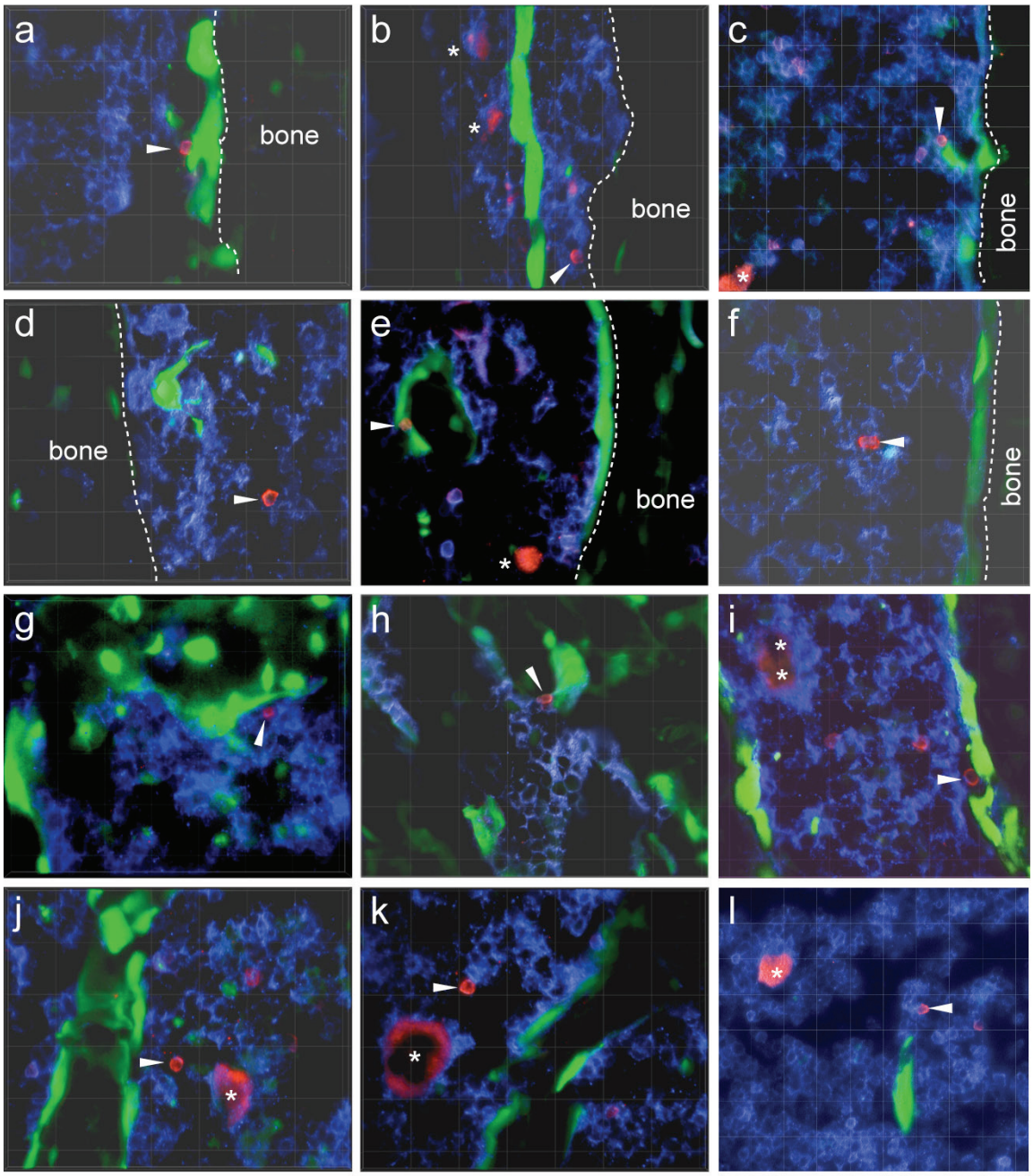

Supplementary Figure 7. HSCs are localized near Nes:GFP$^+$ cells in the bone marrow. Immunostaining for CD150 (red), CD48 and haematopoietic lineage markers (blue) in femoral sections of *Nes-Gfp* transgenic mice. Examples of CD150$^+$ CD48$^-$ Lin$^-$ HSCs are indicated by arrowheads. HSCs were frequently localized (**a**, **c**) adjacent or (**b**, **d**) close to Nes:GFP$^+$ cells near the endosteum, and mostly (**e**, **g**-**i**) in direct contact with or (**j**-**l**) near Nes:GFP$^+$ cells surrounding blood vessels. Asterisks indicate CD150$^+$ Lin / CD48$^+$ megakaryocytes, that can be identified by their large size and characteristic CD150 staining pattern. Grid, 50 μm.

In the histological studies performed, a total number of 42 CD150$^+$ CD48$^-$ Lin$^-$ HSC-enriched cells were identified over several femoral sections, and 37 of them were localized within 50 μm from Nes:GFP$^+$ cells.

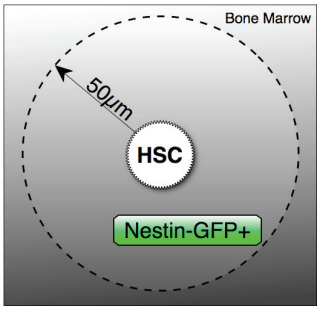

Cell type	Percentage of BM nucleated cells
CD150$^+$ CD48$^-$ Lin$^-$	0.0084 ± 0.0028 % [1]
Nes:GFP$^+$	0.08 ± 0.01 %

The probability of k Nes:GFP$^+$ cells existing within an area (A) with a mean occurrence (λ) is given by the Poisson distribution:

$$Px(X = k) = e^{-\mu}\mu^k/k!$$

where the parameter μ represents the number of expected cells in the sampling area (A):

$$\mu = \lambda * A$$

λ was measured as 5.3 ± 0.8 Nes:GFP$^+$ cells per mm^2 (77.3 ± 11.7 Nes:GFP$^+$ cells in an area of 14.62 ± 0.24 mm^2). The total sampling area (A) is the sum of 100 μm-diameter circles centered on 42 CD150$^+$ CD48$^-$ Lin$^-$ cells:

$$A = 42 * \pi * (50 * 10^{-3}mm)^2 = 0.3297mm^2$$

The number of Nes:GFP$^+$ cells expected in the sampling area is therefore μ = 1.75. The probability of co-localization follows a Poisson distribution shown below. A one-sample inference for the Poisson distribution (small-sample test, p-value method) conclusively shows that the observed frequency of co-localization between CD150$^+$ CD48$^-$ Lin$^-$ and Nes:GFP$^+$ cells is statistically significant ($p < 10^{-16}$).

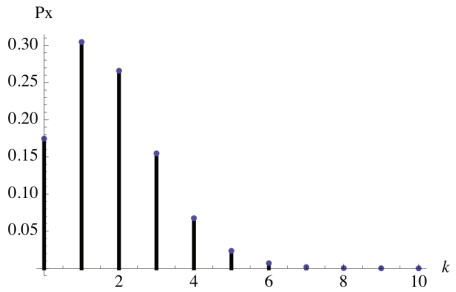

$$H_0 : \mu = \mu_0$$
$$H_1 : \mu \neq \mu_0$$
$$pvalue = min[2 * (1 - \sum_{k=0}^{x-1} \frac{e^{-\mu_0}\mu_0^k}{k!}), 1]$$
$$p = 2 * \left(1 - \sum_{k=0}^{36} (e\text{^}(-1.75)(1.75)\text{^}k)/(k!)\right)$$
$$p < 1 * 10^{-16}$$

Supplementary Figure 8. **The physical association of GFP$^+$ and CD150$^+$ CD48$^-$ Lin$^-$ cells in the bone marrow of *Nes-Gfp* transgenic mice is statistically significant**.

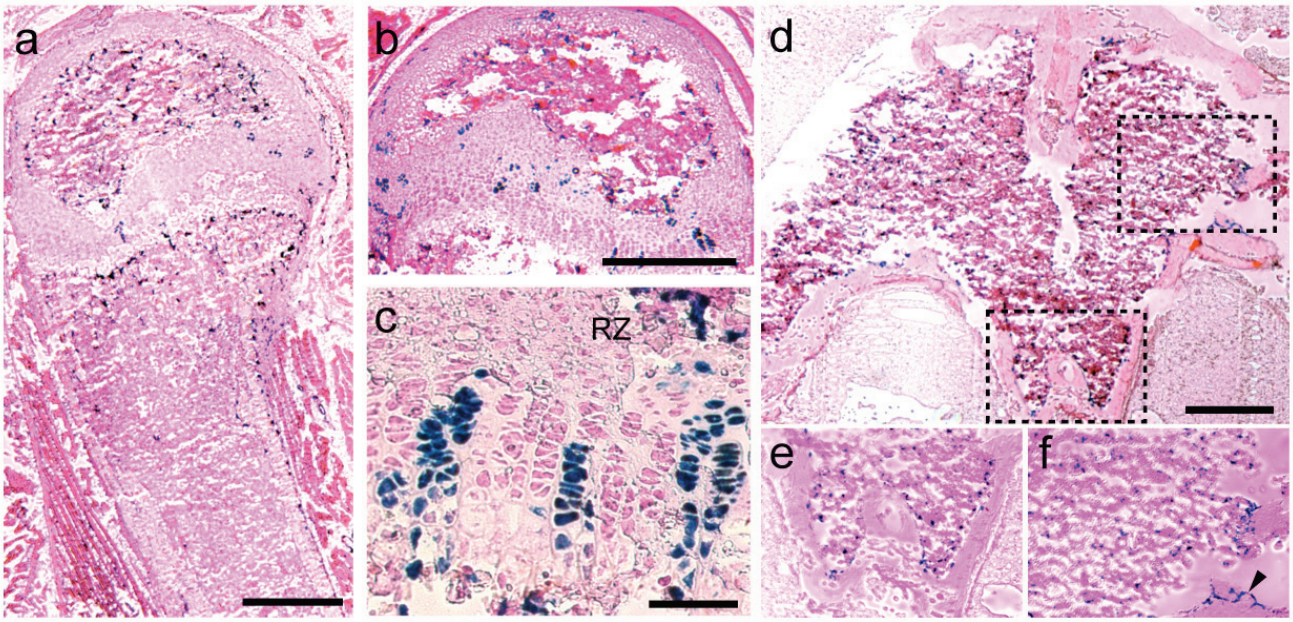

Supplementary Figure 9. **Nestin$^+$ cells contribute to osteochondral lineages**. Lineage tracing studies using *Nes-Cre* mice bred to the *R26R* reporter line have demonstrated the contribution of nestin$^+$ cells to bone and cartilage formation. **a**-**c**, Longitudinal sections of the femur of a 4 week-old mouse showing the presence of cells derived from nestin$^+$ cells in the bone marrow, with higher abundance in the trabecular region, and their contribution to endochondral ossification by derivation into osteoblasts and chondrocytes. Numerous chondrocytes and osteoblasts derived from nestin$^+$ cells can be observed in the reserve zone (RZ) and lining the trabecular bone surface, respectively. **c**, Columnar proliferating and hypertrophying chondrocytes derived from nestin$^+$ cells, shown in the growth plate at higher magnification. **d**-**f**, Horizontal section of the frontal bone of the skull of a 4 week-old mouse showing the contribution of nestin$^+$ cells in intramembranous ossification. Numerous osteoblasts and osteocytes (**f**, arrowhead) derived from nestin$^+$ cells can be observed in the frontal bone. Dashed rectangles (**d**) are shown below at higher magnification (**e**-**f**). Bar scale,100 μm (**c**); 500 μm (**a**-**b**, **d**).

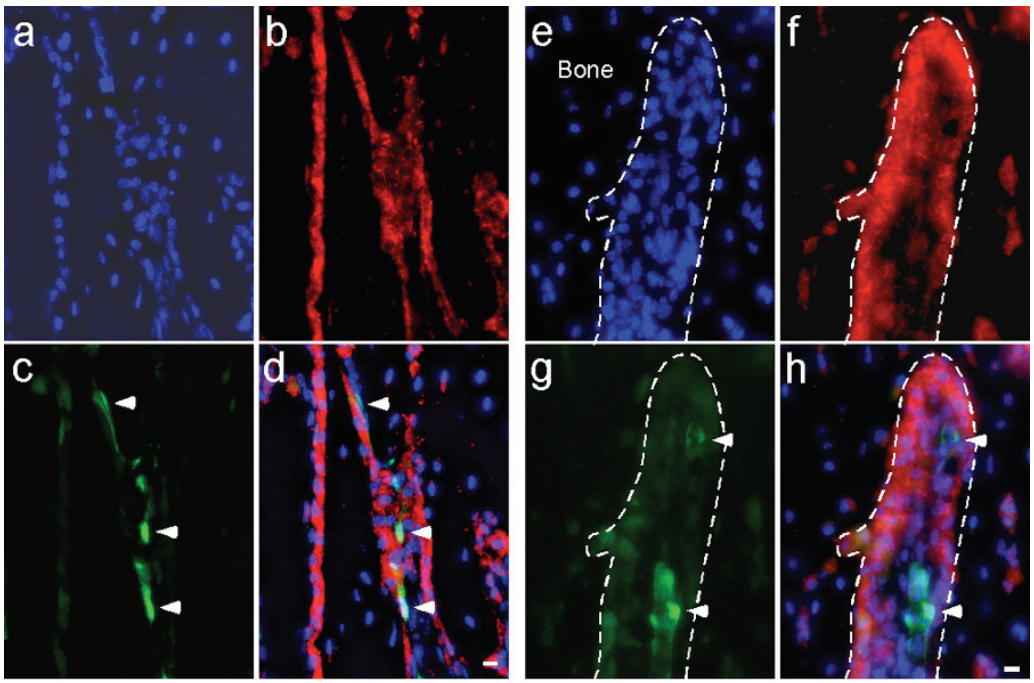

Supplementary Figure 10. **N-cadherin expression in femoral sections from *Nes-Gfp* transgenic mice**. Immunostaining for N-cadherin using a rabbit polyclonal antibody was performed as described[10]. Two illustrative Z-stacks (**a**-**d** and **e**-**f**) are shown. Individual fluorescence for DAPI (**a**, **e**, blue), N-cadherin (**b**, **f**, red), GFP (**c**, **g**, green) and the merged images (**d**, **h**) are shown for comparison. Like osterix$^+$ cells (please see main paper), N-cadherin$^+$ cells were much more abundant than Nes:GFP$^+$ cells in the trabecular bone marrow, and were localized between Nes:GFP$^+$ cells and the bone surface. GFP+ cells with the typical morphology and distribution of Nes:GFP$^+$ cells are indicated with arrowheads, and were very different from N-cadherin$^+$ osteoblastic cells. **e**-**h**, Bone margins are indicated with dashed lines. Bar scale,10 μm.

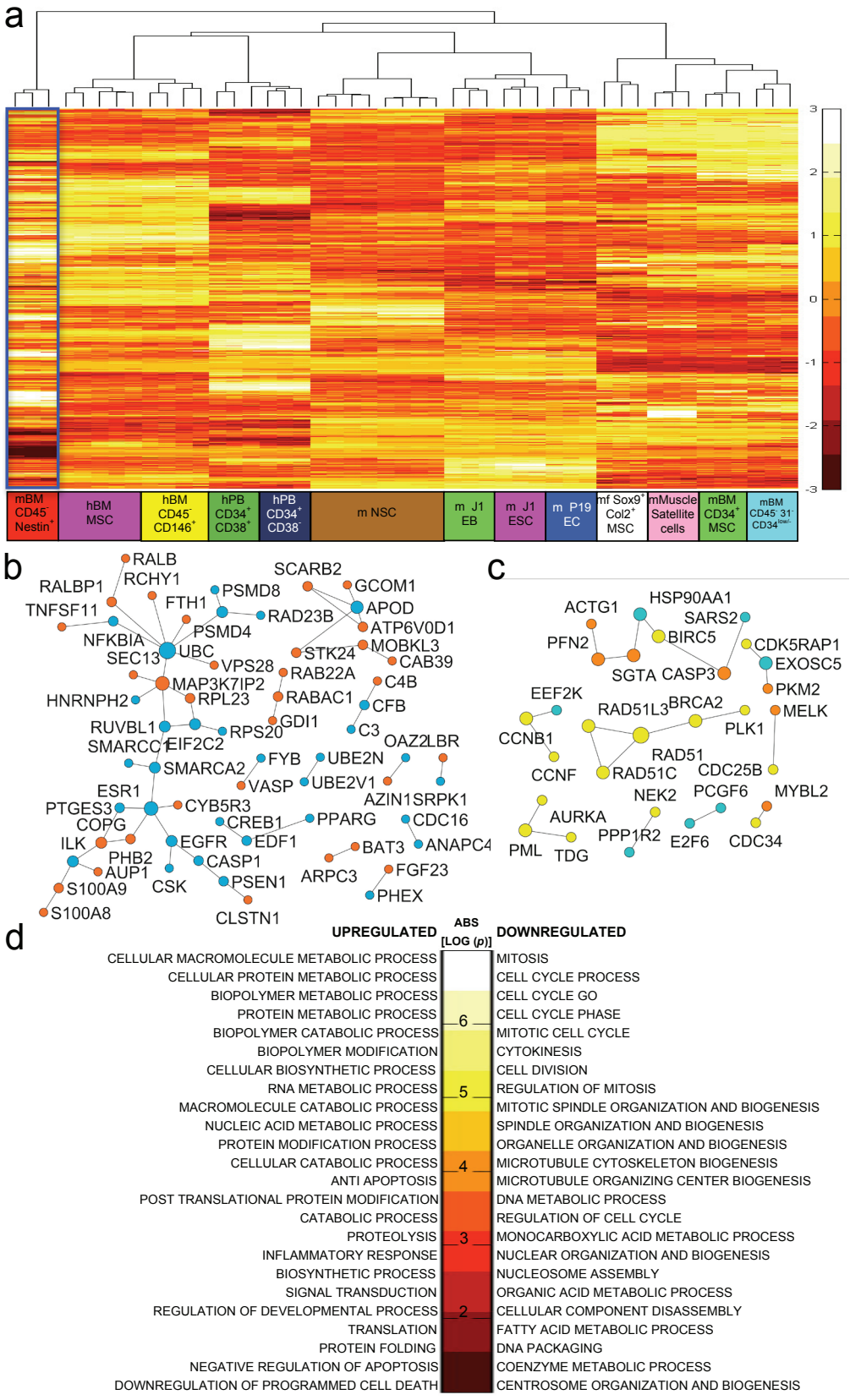
a
mBM CD45- Nestin+
hBM MSC
hBM CD45- CD146+
hPB CD34+ CD38+
hPB CD34+ CD38-
m NSC
m J1 EB
m J1 ESC
m P19 EC
mf Sox9+ Col2+ MSC
mMuscle Satellite cells
mBM CD34+ MSC
mBM CD45- 31- CD34low-
3
2
1
0
-1
-2
-3
b
RALB
RCHY1
RALBP1
SCARB2
GCOM1
PSMD8
FTH1
TNFSF11
RAD23B
APOD
ATP6V0D1
PSMD4
NFKBIA
MOBKL3
UBC
SEC13
STK24
CAB39
VPS28
RAB22A
MAP3K7IP2
C4B
HNRNPH2
RPL23
RABAC1
CFB
GDI1
RUVBL1
RPS20
C3
SMARCC1
EIF2C2
OAZ2LBR
SMARCA2
FYB
UBE2N
VASP
UBE2V1
ESR1
AZIN1
SRPK1
PTGES3
CYB5R3
COPG
CREB1
PPARG
CDC16
ILK
EGFR
EDF1
BAT3
ANAPC4
PHB2
CASP1
AUP1
ARPC3
FGF23
CSK
PSEN1
S100A9
PHEX
S100A8
CLSTN1
c
ACTG1
HSP90AA1
SARS2
PFN2
BIRC5
CDK5RAP1
EXOSC5
SGTA
CASP3
PKM2
EEF2K
RAD51L3
BRCA2
MELK
CCNB1
PLK1
RAD51
CCNF
RAD51C
CDC25B
NEK2
PCGF6
MYBL2
AURKA
PML
TDG
PPP1R2
E2F6
CDC34
d
UPREGULATED
ABS [LOG (p)]
DOWNREGULATED
CELLULAR MACROMOLECULE METABOLIC PROCESS
CELLULAR PROTEIN METABOLIC PROCESS
BIOPOLYMER METABOLIC PROCESS
PROTEIN METABOLIC PROCESS
BIOPOLYMER CATABOLIC PROCESS
BIOPOLYMER MODIFICATION
CELLULAR BIOSYNTHETIC PROCESS
RNA METABOLIC PROCESS
MACROMOLECULE CATABOLIC PROCESS
NUCLEIC ACID METABOLIC PROCESS
PROTEIN MODIFICATION PROCESS
CELLULAR CATABOLIC PROCESS
ANTI APOPTOSIS
POST TRANSLATIONAL PROTEIN MODIFICATION
CATABOLIC PROCESS
PROTEOLYSIS
INFLAMMATORY RESPONSE
BIOSYNTHETIC PROCESS
SIGNAL TRANSDUCTION
REGULATION OF DEVELOPMENTAL PROCESS
TRANSLATION
PROTEIN FOLDING
NEGATIVE REGULATION OF APOPTOSIS
DOWNREGULATION OF PROGRAMMED CELL DEATH
6
5
4
3
2
MITOSIS
CELL CYCLE PROCESS
CELL CYCLE GO
CELL CYCLE PHASE
MITOTIC CELL CYCLE
CYTOKINESIS
CELL DIVISION
REGULATION OF MITOSIS
MITOTIC SPINDLE ORGANIZATION AND BIOGENESIS
SPINDLE ORGANIZATION AND BIOGENESIS
ORGANELLE ORGANIZATION AND BIOGENESIS
MICROTUBULE CYTOSKELETON BIOGENESIS
MICROTUBULE ORGANIZING CENTER BIOGENESIS
DNA METABOLIC PROCESS
REGULATION OF CELL CYCLE
MONOCARBOXYLIC ACID METABOLIC PROCESS
NUCLEAR ORGANIZATION AND BIOGENESIS
NUCLEOSOME ASSEMBLY
ORGANIC ACID METABOLIC PROCESS
CELLULAR COMPONENT DISASSEMBLY
FATTY ACID METABOLIC PROCESS
DNA PACKAGING
COENZYME METABOLIC PROCESS
CENTROSOME ORGANIZATION AND BIOGENESIS

e

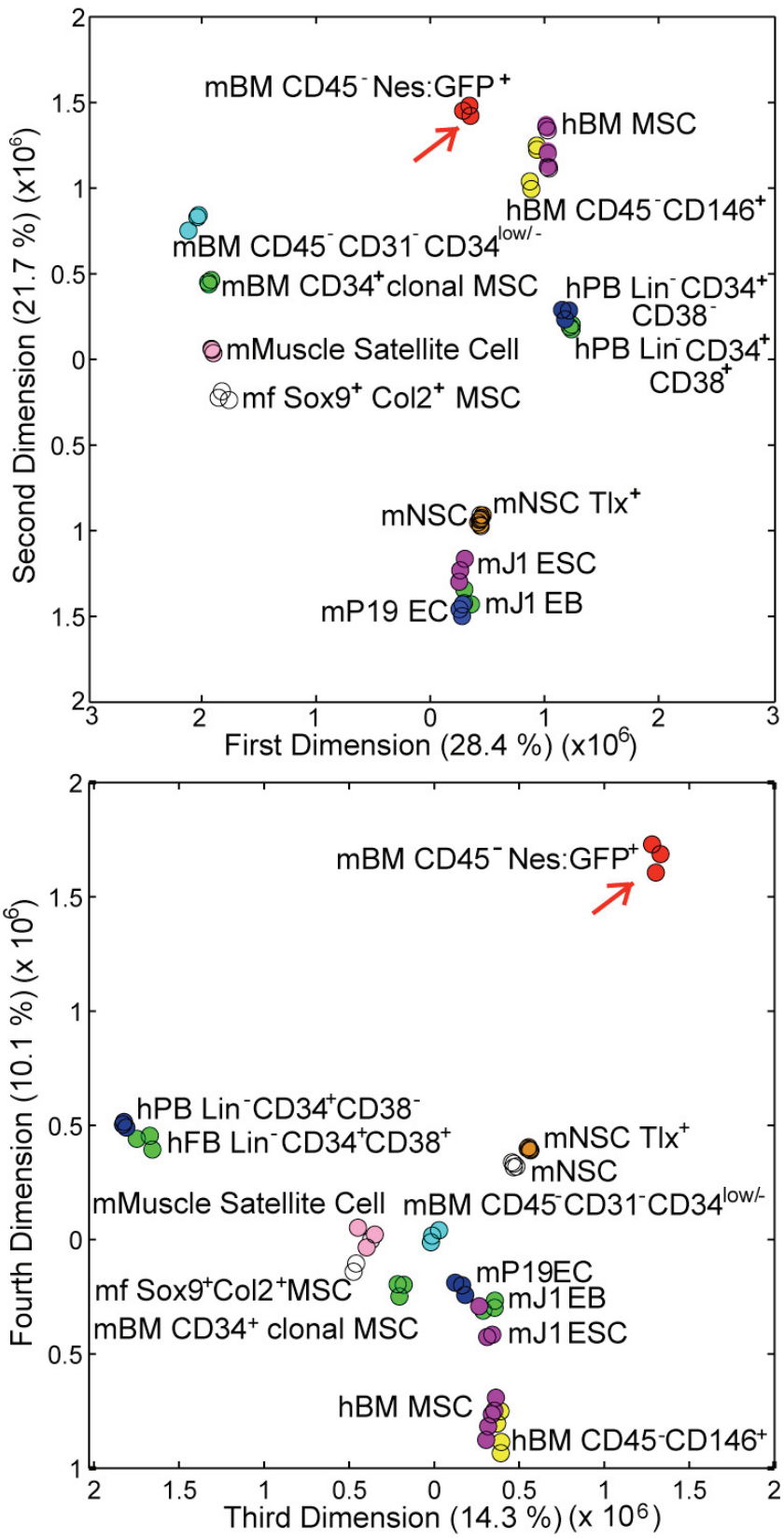
mBM CD45⁻ Nes:GFP⁺
hBM MSC
hBM CD45⁻CD146⁺
mBM CD45⁻ CD31⁻ CD34low/-
mBM CD34⁺clonal MSC
hPB Lin⁻ CD34⁺ CD38⁻
mMuscle Satellite Cell
hPB Lin⁻CD34⁺ CD38⁺
mf Sox9⁺ Col2⁺ MSC
mNSC
mNSC Tlx⁺
mJ1 ESC
mP19 EC
mJ1 EB
Second Dimension (21.7 %) (x10⁶)
First Dimension (28.4 %) (x10⁶)
mBM CD45⁻ Nes:GFP⁺
hPB Lin⁻CD34⁺CD38⁻
hFB Lin⁻CD34⁺CD38⁺
mNSC Tlx⁺
mNSC
mMuscle Satellite Cell
mBM CD45⁻CD31⁻CD34low/-
mf Sox9⁺Col2⁺MSC
mP19EC
mJ1 EB
mBM CD34⁺ clonal MSC
mJ1 ESC
hBM MSC
hBM CD45⁻CD146⁺
Fourth Dimension (10.1 %) (x 10⁶)
Third Dimension (14.3 %) (x 10⁶)

f

	Experiment
1	GSM545815 mBM CD45$^-$Nes:GFP$^+$
2	GSM545816 mBM CD45$^-$ Nes:GFP$^+$
3	GSM545817 mBM CD45$^-$ Nes:GFP$^+$
4	GSM314045 mNSC
5	GSM314046 mNSC
6	GSM314047 mNSC
7	GSM314048 mNSC
8	GSM148485 hBM CD45$^-$ CD146$^+$
9	GSM148487 hBM CD45$^-$ CD146$^+$
10	GSM148488 hBM CD45$^-$ CD146$^+$
11	GSM148491 hBM CD45$^-$ CD146$^+$
12	GSM87697 hFB Lin$^-$ CD34$^+$ CD38$^+$
13	GSM87693 hFB Lin$^-$ CD34$^+$ CD38$^+$
14	GSM87695 hFB Lin$^-$CD34$^+$ CD38$^+$
15	GSM86779 hPB Lin$^-$ CD34$^+$ CD38$^-$
16	GSM86781 hPB Lin$^-$CD34$^+$ CD38$^-$
17	GSM86783-4 hPB Lin$^-$ CD34$^+$ CD38$^-$
18	GSM72616 J1-EB
19	GSM72618 J1-EB
20	GSM72621 J1-EB
21	GSM93543 P19
22	GSM93541 P19
23	GSM93545 P19
24	GSM86489 mBM CD45$^-$ CD31$^-$ CD34$^{low/-}$
25	GSM86492 mBM CD45$^-$ CD31$^-$ CD34$^{low/-}$
26	GSM86495 mBM CD45$^-$ CD31$^-$ CD34$^{low/-}$
27	GSM86435 mBM CD34$^+$ clonal MSC
28	GSM86438 mBM CD34$^+$ clonal MSC
29	GSM86441 mBM CD34$^+$ clonal MSC
30	GSM86510 mf Sox9$^+$ Col2$^+$ MSC
31	GSM86504 mf Sox9$^+$ Col2$^+$ MSC
32	GSM86507 mf Sox9$^+$Col2$^+$ MSC
33	GSM73026 mMuscle Satellite Cell
34	GSM73029 mMuscle Satellite Cell
35	GSM73032 mMuscle Satellite Cell
36	GSM72622 J1-ESC
37	GSM72624 J1-ESC
38	GSM72626 J1-ESC
39	GSM194075 hBM MSC
40	GSM194076 hBM MSC
41	GSM194077 hBM MSC
42	GSM194078 hBM MSC
43	GSM194079 hBM MSC
44	GSM252290 mNSC
45	GSM252291 mNSC
46	GSM252292 mNSC
47	GSM252296 mNSC

Supplementary Figure 11. **Molecular signature of bone marrow Nestin $^+$ cells**. Genome–wide expression profile of BM CD45$^-$ Nes:GFP$^+$ cells compared to multiple stem cells obtained from Gene Expression Omnibus (http://www.ncbi.nlm.nih.gov/geo/) and the stem-base database (http://www.stembase.ca/?path=/), including mouse MSCs (mBM CD34$^+$, mf Sox9$^+$ Col2$^+$ MSCs and mBM CD45$^-$ CD31$^-$ CD34$^{low/-}$) and human MSCs (hBM MSC, hBM CD45$^-$ CD146$^+$), mouse embryonic (mJ1ESC, mJ1EB) and mouse neural stem cells (mNSC), mouse pluripotent embryonal carcinoma cells (mP19EC), muscle satellite cells and human peripheral blood haematopoietic stem and progenitor cells (hPB CD34$^+$ CD38$^-$ and CD34$^+$ CD38$^-$; please see Supplementary Fig. 11b for a complete list with accesion numbers). **a**, Hierarchical clustering; the group of BM CD45$^-$ Nes:GFP$^+$ cells, including 3 biological replicates containing two adult *Nes-Gfp* of different gender each, is marked with a blue square. **b**-**d**, Gene Ontology analysis of genes differentially expressed in BM CD45$^-$ Nes:GFP$^+$ cells. **c**-**d**, Protein-protein interactions from (**c**) up- and (**d**) down-regulated genes. **d**, Enrichment of Gene Ontology terms for Biological Processes. **e**, Principal coordinates analysis of gene expression across all experimental groups. Principal coordinates analysis was conducted on the most variable (top 10 % = 948) ranked genes using the Manhattan (city block) distance metric and the Matlab Statistics Toolbox. Data reconstruction in the first four principal coordinates (accounting for ~ 80% total variation) is shown. **f**, List of microarray experiments with accession numbers; m, mouse; f, fetal; BM, bone marrow; NSC, neural stem cell; h, human; FB, fetal blood; PB, peripheral blood; EB, embryoid bodies; MSC, mesenchymal stem cell; ESC, embryonic stem cell.

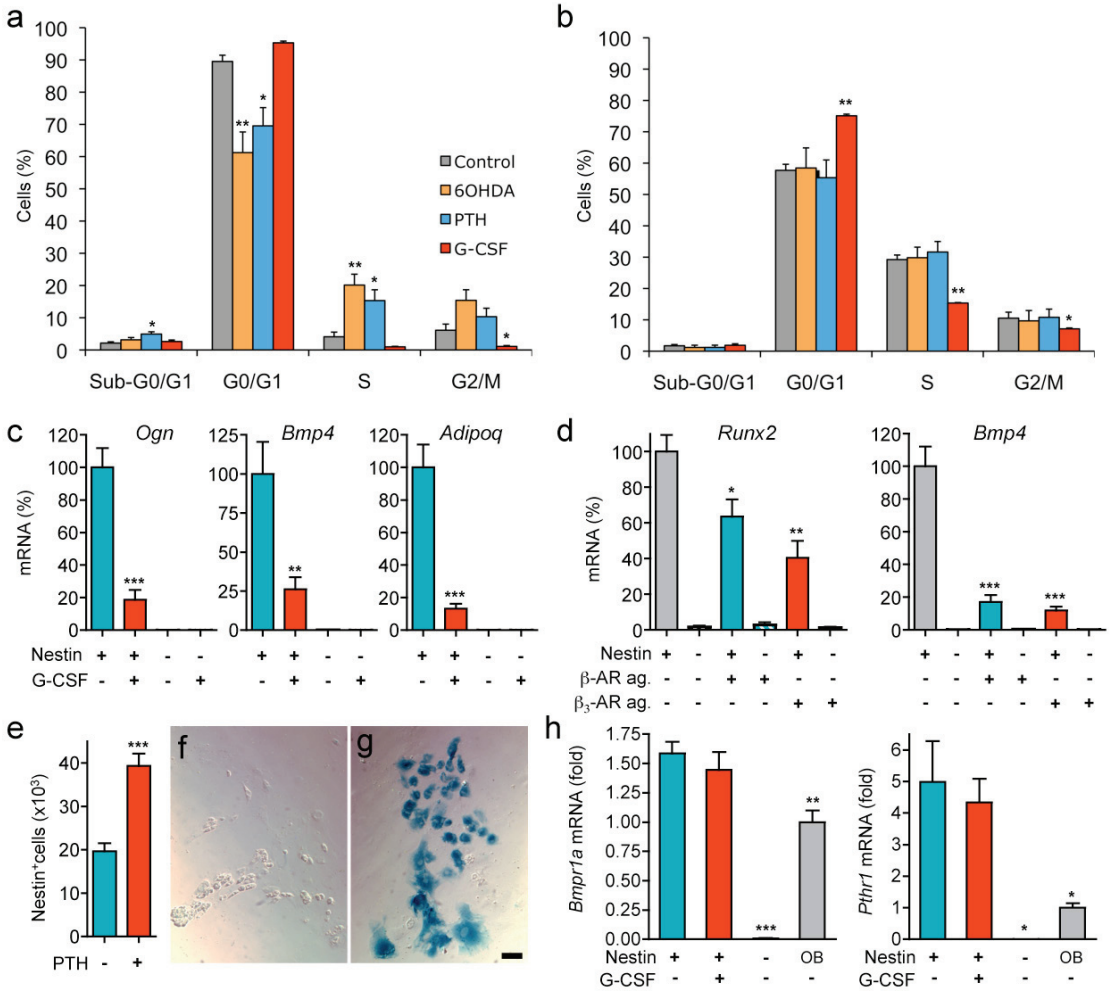

Supplementary Figure 12. Proliferation and differentiation of bone marrow Nes:GFP$^+$ MSCs are regulated by hormones, cytokines and the sympathetic nervous system.
a-**b**, Cell cycle profile of (**a**) CD45$^-$ GFP$^+$ and (**b**) CD45$^-$ GFP$^-$ cells sorted from the bone marrow of *Nes-Gfp* transgenic mice chemically sympathectomized (6OHDA), treated with parathormone (PTH) for 10 days, injected with G-CSF or vehicle (as described in the Methods). Cells were harvested and fixed for > 2h at 4ºC in 70% Ethanol and stained with a solution containing 0.2 mg ml^{-1} DNAse-free RNase A, 0.1% Triton X-100 and 20 μg ml^{-1} Propidium iodide in PBS. Nes:GFP$^+$ cells (**a**) are much more quiescent (90% G0/G1, 10% S/G2/M) than the remaining CD45$^-$ cells (**b**) but are selectively induced to proliferate by parathormone over 10 days (70% G0/G1, 26% S/G2/M) or by chemical sympathectomy (61% G0/G1, 36% S/G2/M). G-CSF reduced proliferation of both (**a**) CD45$^-$ Nes:GFP$^+$ (95% G0/G1, 2% S/G2/M) and (**b**) CD45$^-$ Nes:GFP$^-$ (75% G0/G1, 22% S/G2/M) cells (n = 4-5). **c**, G-CSF selectively and significantly downregulated in CD45$^-$ Nes:GFP$^+$ cells genes involved in osteoblastic (osteoglycin, *Ogn*; bone morphogenetic protein-4, *Bmp4*) and adipogenic (adiponectin, *Adipoq*) differentiation, whose expression was 650 to 1325-fold higher in Nes:GFP$^+$ cells than in the rest of the bone marrow CD45$^-$ population (n = 6). **d**, Activation of β_3-AR significantly downregulated osteoblastic differentiation genes (*Runx2* and *Bmp4*) in BM CD45$^-$ Nes:GFP$^+$ cells. Animals were injected 2 h before harvest with saline, a non-selective β- (isoproterenol, β-AR) or a selective β_3-AR (BRL37344) (2 mg kg^{-1}, i.p.). Stimulation of the β_3-AR significantly downregulated these genes in Nes:GFP$^+$ cells but not in the remaining bone marrow CD45$^-$ population (n = 6). **e**-**g**, Daily administration of parathormone (80 μg kg^{-1}; i.p.) over 5 weeks (**e**) doubled the number of CD45$^-$ Nes:GFP$^+$ cells in the bone marrow and primed them to differentiate into osteoblasts identified by *Col2.3*-driven β-galactosidase expression (**g**; n = 4). **f**-**g**, Representative examples of CD45$^-$ Nes:GFP$^+$ cells sorted from the bone marrow of mice injected with (**g**) parathormone or (**f**) saline as described[3], and plated for one week in osteoblastic differentiation medium (n = 4). Bar scale, 100 μm. **h**, Expression of type IA bone morphogenetic protein receptor (*Bmpr1a*) and parathormone receptor-1 (*Pthr1*) was significantly higher in CD45$^-$ Nes:GFP$^+$ cells than in CD45$^-$ Nes:GFP$^-$ cells or primary osteoblasts. The expression of these receptors in CD45$^-$ Nes:GFP$^+$ cells was not affected significantly by G-CSF treatment (n = 3). **c**-**d**, **h**, Quantitative real-time RT-PCR was performed in RNA samples from primary osteoblasts and from CD45$^-$ GFP$^+$ and CD45$^-$ GFP$^-$ cells sorted from the bone marrow of *Nes-Gfp* transgenic mice. Unpaired two-tailed *t* test. * $p < 0.05$, ** $p < 0.01$, *** $p < 0.001$. Error bars indicate standard error.

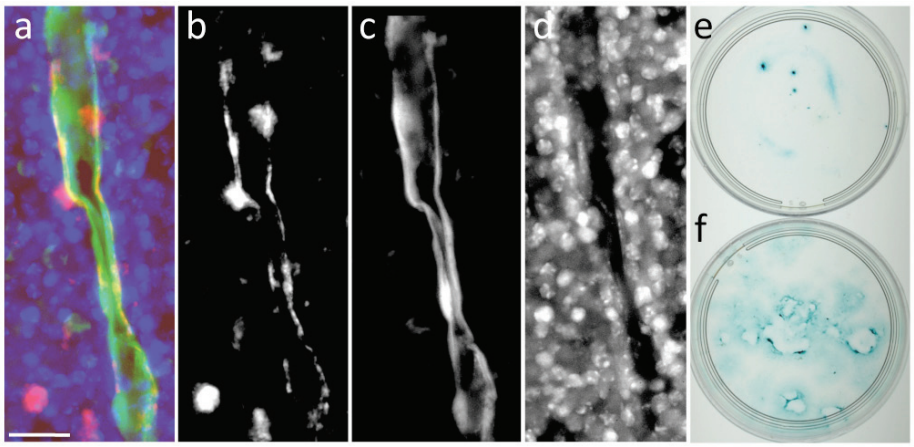

Supplementary Figure 13. **Bone marrow Nes:GFP$^+$ cells have parathormone receptor and respond to parathormone *in vitro* by proliferating and differentiating into osteoblasts**.
a-**d**, Immunofluorence of trabecular bone marrow from adult *Nes-Gfp* transgenic mouse showing the presence of parathormone receptor-1 (PTHR1, red) on putative osteoblastic cells and also on the surface of GFP$^+$ peri-vascular cells (green). A rabbit polyclonal anti-PTHR1 antibody (1:100, Abcam) was detected using the TSA amplification system (red; PerkinElmer). Nuclei were stained with DAPI (blue). Bar scale, 50 μm. **b**-**d**, Individual fluorescence signals for PTHR1 (**b**), GFP (**c**) and DAPI (**d**) are also shown for comparison. Note the proximity of osteoblasts and Nes:GFP$^+$ cells in the trabecular bone marrow. **e**-**f**, Increased *in vitro* proliferation and osteoblastic differentiation after PTH treatment. An equal number of CD45$^-$ GFP$^+$ cells were sorted from the bone marrow of *Nes-Gfp* / *Col2.3-Cre* / *R26R* triple-transgenic mice and cultured for 4 weeks in sphere-forming conditions (as described in the Methods) with a basic combination of growth factors (FGFb, IGF-1, EGF) with (**f**) or without (**e**) the addition of rat PTH 1-34 (Bachem. Bioscience; 50 ng ml^{-1}). Culture dishes were fixed and stained for X-gal as described in the Methods. Note the increased number of Col2.3$^+$ (blue deposits) osteoblasts derived from Nes:GFP$^+$ cells in the presence of parathormone (**f**).

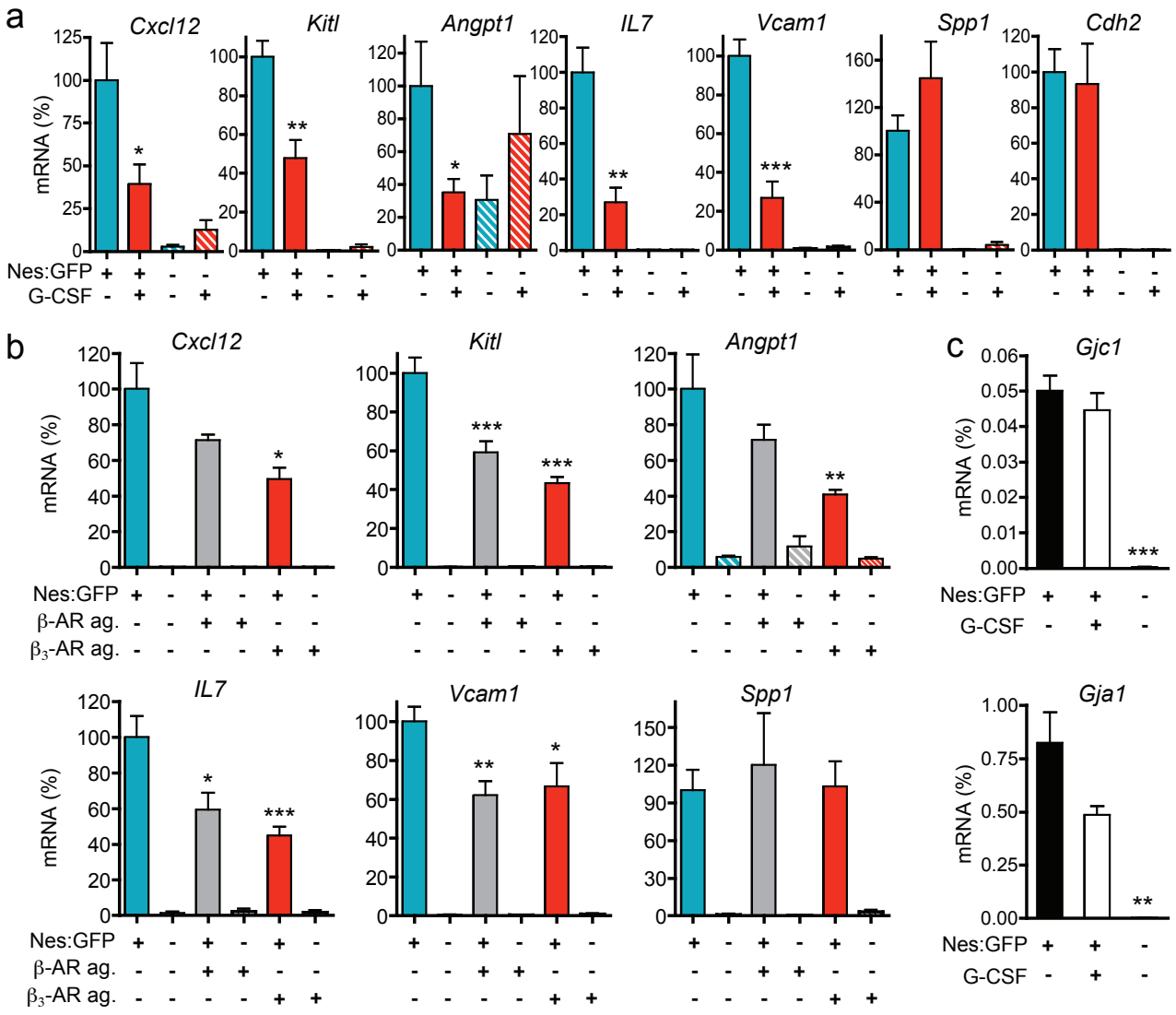

Supplementary Figure 14. **Expression of HSC maintenance genes in bone marrow Nes:GFP$^+$ cells is regulated by the SNS**.

a, Activation of β_3-AR on bone marrow CD45$^-$ Nes:GFP$^+$ cells reduced the expression of core HSC maintenance genes. Quantitative real-time RT-PCR was performed in RNA samples from CD45$^-$ GFP$^+$ and CD45$^-$ GFP$^-$ cells sorted from the bone marrow of *Nes-Gfp* transgenic mice injected 2h before harvest with saline, a non-selective β- (isoprenaline, β-AR) or a selective β_3-AR agonist (BRL37344; β_3-AR) (2 mg kg^{-1}, i.p., n = 6). **b**, Expression of Connexin-45 (Gjc1) and Connexin-43 (Gja1) was 200 to 500-fold higher in Nes:GFP$^+$ cells than in the remaining bone marrow CD45$^-$ population (n = 3). * $p < 0.05$, ** $p < 0.01$, *** $p < 0.001$; unpaired two-tailed *t* test. Error bars indicate SEM.

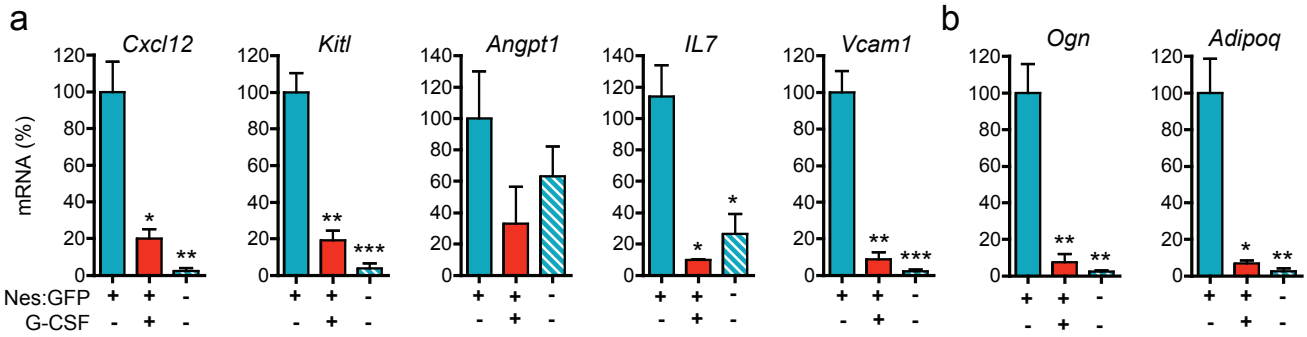

Supplementary Figure 15. **Repetition of Q-PCR experiments using *β-actin* instead of *Gapdh* as a housekeeping gene**.
a-**b**, Quantitative real-time RT-PCR was performed in RNA samples from CD45$^-$ GFP$^+$ and CD45$^-$ GFP$^-$ cells sorted from the bone marrow of *Nes-Gfp* transgenic mice. Very reproducible results were obtained using β-*actin* instead of *Gapdh* as a housekeeping gene. Core genes involved in (**a**) HSC maintenance in the bone marrow and (**b**) differentiation towards mesenchymal lineages were highly expressed in Nes:GFP$^+$ cells compared to the remaining stromal population, and were significantly downregulated after G-CSF treatment (n = 3-7). * $p < 0.05$, ** $p < 0.01$, *** $p < 0.001$; unpaired two-tailed *t* test. Error bars indicate SEM.

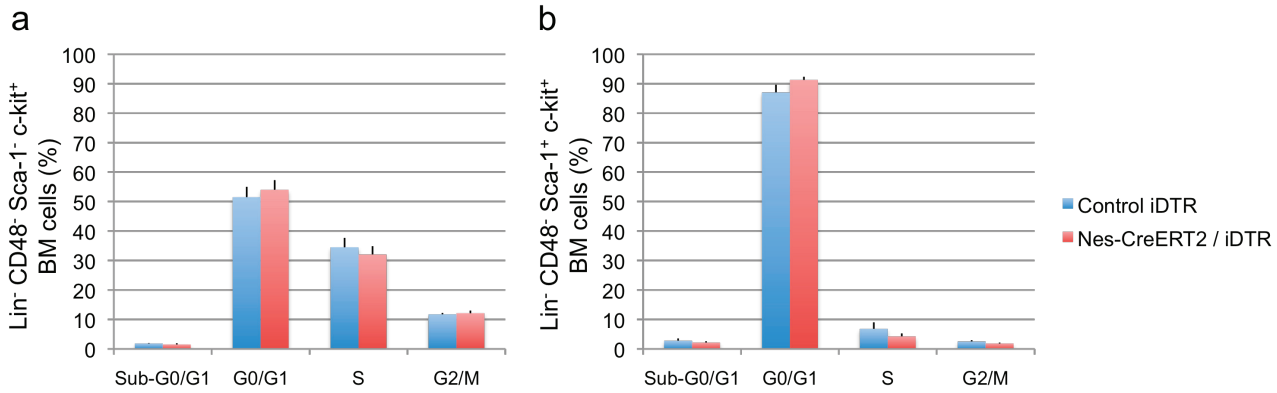

Supplementary Figure 16. **Selective depletion of nestin^{+} cells in adult *Nes-Cre^{ERT2}* / *iDTR* mice does not affect the cell cycle or apoptosis of haematopoietic stem and progenitor cells**. Cell cycle profile of (**a**) Lin^{-} CD48^{-} Sca-1^{-} c-kit^{+} haematopoietic progenitors and (**b**) Lin^{-} CD48^{-} Sca-1^{+} c-kit^{+} HSC-enriched cells sorted from the bone marrow of 6 to 12-week old *Nes-Cre^{ERT2}* / *iDTR* double- and control *iDTR* single-transgenic mice 16 days after tamoxifen and diphtheria toxin treatment. Cells were harvested and fixed for > 2h at 4º C in 70% ethanol and stained with a solution containing 0.2 mg ml^{-1} DNAse-free RNase A, 0.1% Triton X-100 and 20 μg ml^{-1} Propidium iodide (Sigma) in PBS. No differences were observed in the frequencies of apoptotic (Sub-G0/G1) cells or in cell cycle profiles between the two groups of animals (n = 4-6). Unpaired two-tailed *t* test. Error bars indicate SEM.

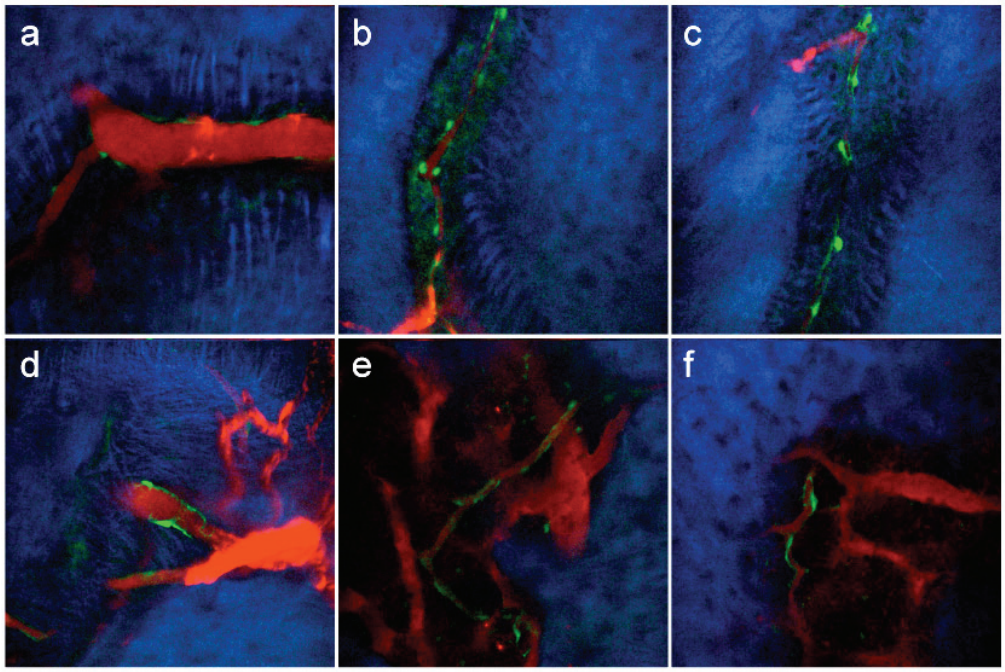

Supplementary Figure 17. **Calvarial bone marrow Nes:GFP$^+$ cells are peri-vascular**.
In vivo imaging of the calvarium of *Nes-Gfp* transgenic mice i.v. injected with Qdot (Invitrogen, red). **a**-**c**, Nes:GFP$^+$ (green) cells surrounding blood vessels in the coronal suture. **d**-**f**, Peri-vascular Nes:GFP$^+$ cells in the endosteal region. The blue fluorescence corresponds to second harmonic signal generated by bone collagen when illuminated by femtosecond titanium:sapphire laser pulses, as previously described[40].

Supplementary Table 1.

Mouse #	X-gal$^-$ and Oil Red O$^-$	X-gal$^+$ and Oil Red O$^-$	X-gal$^+$ and Oil Red O$^+$	Total
1	11	142	102	255
2	15	130	94	239
3	6	77	61	144
4	7	43	30	80
5	0	70	30	100
6	4	66	51	121

Supplementary Table 1. Multipotency of Nes:GFP$^+$ secondary mesenspheres. Heterotopic bone ossicles loaded with individual clonal spheres obtained from *Nes-Gfp / Col2.3-Cre / R26R* triple-transgenic mice were harvested two months after their subcutaneous implantation into littermates that did not carry the transgenes and enzymatically digested. Secondary spheres were cultured in the same conditions as primary spheres. After three weeks, the cultures were fixed and stained with X-gal and Oil Red O, as described in the Methods. The number of spheres X-gal$^-$ Oil Red O$^-$, X-gal$^+$ Oil Red O$^-$ and X-gal$^+$ Oil Red O$^+$, and the total number of spheres analyzed from each mouse are shown in the Table.

Supplementary Table 2. Sequence of oligonucleotides used for quantitative real-time RT-PCR.

Primers	Sequence	Product (bp)	Annealing (°C)
*Cxcl12*_Fw	CGCCAAGGTCGTCGCCG		
*Cxcl12*_Rv	TTGGCTCTGGCGATGTGGC	118	60
*Adrb3*_Fw	TGCGCACCTTAGGTCTCATTATGG		
*Adrb3*_Rv	AAACTCCGCTGGGAACTAGAGAGG	110	60
*Gfp*_Fw	ATCATGGCCGACAAGCAGAAGAAC		
*Gfp*_Rv	GTACAGCTCGTCCATGCCGAGAGT	280	60
*Kitl*_Fw	CCCTGAAGACTCGGGCCTA		
*Kitl*_Rv	CAATTACAAGCGAAATGAGAGCC	65	60
*Angpt1*_Fw	CTCGTCAGACATTCATCATCCAG		
*Angpt1*_Rv	CACCTTCTTTAGTGCAAAGGCT	138	60
*IL7*_Fw	GTGCTGCTCGCAAGTTGAAG		
*IL7*_Rv	AGTTCACCAGTGTTTGTGTGC	102	60
*Vcam1*_Fw	GACCTGTTCCAGCGAGGGTCTA		
*Vcam1*_Rv	CTTCCATCCTCATAGCAATTAAGGTG	121	60
*Spp1*_Fw	TCCCTCGATGTCATCCCTGTTG		
*Spp1*_Rv	GGCACTCTCCTGGCTCTCTTTG	149	60
*Ogn*_Fw	ACCATAACGACCTGGAATCTGT		
*Ogn*_Rv	AACGAGTGTCATTAGCCTTGC	122	60
*Alpl*_Fw	CACAATATCAAGGATATCGACGTGA		
*Alpl*_Rv	ACATCAGTTCTGTTCTTCGGGTACA	73	60
*Gpnmb*_Fw	CCCCAAGCACAGACTTTTGAG		
*Gpnmb*_Rv	GCTTTCTGCATCTCCAGCCT	65	60
*Runx2*_Fw	TTACCTACACCCCGCCAGTC		
*Runx2*_Rv	TGCTGGTCTGGAAGGGTCC	128	60
*Sp7*_Fw	ATGGCGTCCTCTCTGCTTGA		
*Sp7*_Rv	GAAGGGTGGGTAGTCATTTG	275	60
*Bglap*_Fw	GGGCAATAAGGTAGTGAACAG		
*Bglap*_Rv	GCAGCACAGGTCCTAAATAGT	183	60
*Bmp4*_Fw	TAAGAACTGCCGTCGCCATT		
*Bmp4*_Rv	GGCCACAATCCAATCATTCC	69	60
*Adipoq*_Fw	TGTTCCTCTTAATCCTGCCCA		
*Adipoq*_Rv	CCAACCTGCACAAGTTCCCTT	103	60
*Pparg*_Fw	ACCACTCGCATTCCTTTGAC		
*Pparg*_Rv	TGGGTCAGCTCTTGTGAATG	100	60
*Cfd*_Fw	TGCATCAACTCAGAGTGTCAATCA		
*Cfd*_Rv	TGCGCAGATTGCAGGTTGT	50	60
*Acan*_Fw	CACGCTACACCCTGGACTTTG		
*Acan*_Rv	CCATCTCCTCAGCGAAGCAGT	269	60
*Col11a2*_Fw	TGGCACTCCTGGTCCAGAAG		
*Col11a2*_Rv	GCCGGGCTTTCCTGCTA	120	60
*Col2a1*_Fw	GTGGAGCAGCAAGAGCAAGGA		
*Col2a1*_Rv	CTTGCCCCACTTACCAGTGTG	333	60
*Sox9*_Fw	CAAGCGGAGGCCGAAGA		
*Sox9*_Rv	CAGCTTGCACGTCGGTTT	186	60
Pthr1_Fw	ACCGTGGCTGTGCTCATCCT		
Pthr1_Rv	CCAGCGTGAAGCCAGAGTAG	144	60
Bmpr1a_Fw	AACGCTTGCGGCCAATC		
Bmpr1a_Rv	GAÇATTAGCTTCAAAACTGCTCGAA	72	60
Gjc1_Fw	AGATCCACAACCATTCGACATTT		
Gjc1_Rv	TCCCAGGTACATCACAGAGGG	245	60
Gja1_Fw	AGAACACGGCAAGGTGAAGAT		
Gja1_Rv	TGAACCCATAGATGTACCACTGG	119	60
*Gapdh*_Fw	TGTGTCCGTCGTGGATCTGA		
*Gapdh*_Rv	CCTGCTTCACCACCTTCTTGA	77	60
β-actin_Fw	GCTTCTTTGCAGCTCCTTCGT		
β-actin_Rv	ATCGTCATCCATGGCGAACT	62	60